Knox, D. J. and Duffy, B. R. and McKee, S. and Wilson, S. K. (2017) Squeeze-film flow between a curved impermeable bearing and a flat porous bed. Physics of Fluids, 29 (2). ISSN 1070-6631 , http://dx.doi.org/10.1063/1.4974521

Revised Version of Manuscript #16-0594
Squeeze-film flow between a curved impermeable bearing and a flat porous bed

D. J. Knox, B. R. Duffy, S. McKee, and S. K. Wilson
Department of Mathematics and Statistics, University of Strathclyde,
Livingstone Tower, 26 Richmond Street, Glasgow G1 1XH, United Kingdom
(Dated: 13th May 2016, revised 19th September 2016)

Axisymmetric squeeze-film flow in the thin gap between a stationary flat thin porous bed and a curved impermeable bearing moving under a prescribed constant load is analysed. The unsteady Reynolds equation is formulated and solved for the fluid pressure. This solution is used to obtain the time for the minimum fluid layer thickness to reduce to a given value, and, in particular, the finite time for the bearing and the bed to come into contact. The effect of varying the shape of the bearing and the permeability of the layer is investigated, and, in particular, it is found that both the contact time and the fluid pressure behave qualitatively differently for beds with small and large permeabilities. In addition, the paths of fluid particles initially situated in both the fluid layer and the porous bed are calculated. In particular, it is shown that, unlike in the case of a flat bearing, for a curved bearing there are fluid particles, initially situated in the fluid layer, that flow from the fluid layer into the porous bed and then re-emerge into the fluid layer, and the region in which these fluid particles are initially situated is determined.

I. INTRODUCTION

In our recent study (Knox *et al.*[1]) we gave a detailed analysis of the squeeze-film flow between a flat impermeable surface moving under a prescribed constant load and a flat thin porous bed coating a stationary flat impermeable surface. In particular, in this work we obtained an explicit expression for the finite time it takes for the two surfaces to come into contact and analysed the fluid particle paths in both the fluid layer and the porous bed. Our previous work was motivated by a desire for a better understanding of the biomechanics of the human knee joint. Since the layers of cartilage that coat the femoral condyle and the tibial plateau are elastic as well as porous, they tend to deform to produce an approximately uniform layer of fluid as they are squeezed together (Weekley *et al.*[2]), and hence it was not unreasonable to consider the approach of two *flat* surfaces as a first model for the knee. (See, for example, Knox[3] for further details of previous work on the mathematical modelling of both cartilage and the knee.) However, in addition to the human knee, porous squeeze-film flow is also potentially relevant to a range of other situations, including the engagement of wet porous clutch plates (Wu[4]), wet adhesion (Persson[5,6]), and macromolecule-coated colloids interacting with mucus-coated surfaces (Swavola *et al.*[7]). In these and other contexts the shape of one or both surfaces can play a significant role, and so in the present work we extend the analysis of Knox *et al.*[1] to consider the squeeze-film flow between a *curved* impermeable surface and a flat thin porous bed. Note that essentially the same analysis also applies to the squeeze-film flow between a curved thin porous bed and a flat impermeable surface.

Squeeze-film flow with one or two curved impermeable surfaces has, of course, been considered by many previous authors. For example, in pioneering early work Brenner[8] studied a sphere in a fluid approaching (or retreating from) a flat surface, and Cox and Brenner[9] obtained an asymptotic expansion for the force on the sphere when the ratio of the fluid gap to the sphere radius is small. Subsequently, in an important unifying contribution, Stone[10] considered the squeeze-film flow of a more general smooth curved surface moving towards a flat surface. In particular, he showed that the flatter the surface, the longer it takes to reach a given gap thickness. In addition to the recent work by Knox *et al.*[1], there has also been work on squeeze-film

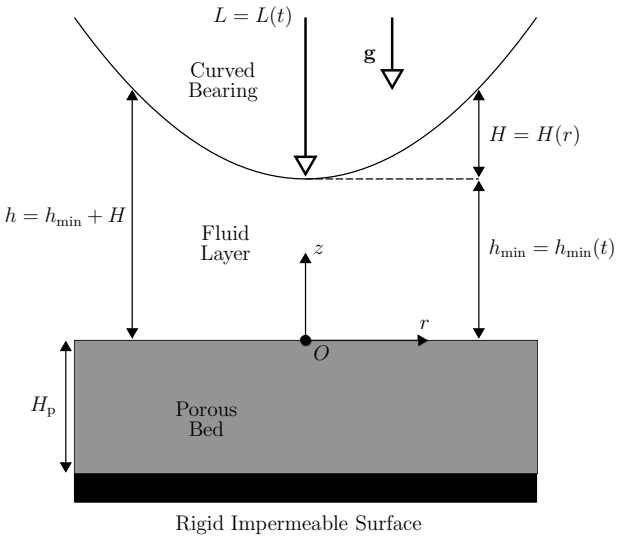

FIG. 1: The geometry of the problem.

flow with one or two porous surfaces by several previous authors. Wu[11] (see also Prakash and Vij[12] and the review by Wu[4]) considered squeeze-film flow between two annular discs, one of which is coated with a porous layer, and found that increasing the permeability of the layer reduces the normal force on the discs. Goren[13] and Nir[14] (see also the summary of previous work given in Table 1 in Ramon *et al.*[15]) calculated the force required to pull a sphere away from contact with a thin porous membrane at a constant velocity, and found that, unlike in the case of an impermeable membrane, the force is finite. In particular, Goren[13] found that the maximum value of the force does not occur when the sphere and the membrane are in contact. More recently, Ramon *et al.*[15] studied a particle with a more general shape approaching a thin porous membrane. They showed that the particle attains a finite non-zero velocity as it sediments under gravity towards the membrane, and hence that it comes into contact with the membrane in a finite time. They also showed that spherical particles would approach the membrane at a greater velocity than flatter particles. Very recently, Majhi *et al.*[16] compared theoretical predictions for the normal force generated in constant-velocity porous squeeze-film flow with experimental results obtained using materials commonly used in the manufacture of composite materials.

The structure of the present work is as follows. The governing equations are derived in Section II and solved (in terms of integrals) in Section III. The behaviour of the minimum fluid layer thickness and contact time, the fluid pressure, and the fluid particle paths and penetration depths are discussed in Sections IV, V and VI, respectively. Asymptotic solutions for the contact time in the limits of small and large permeability are given in Section VII and Appendix A, respectively. Finally, concluding remarks are made in Section VIII.

II. MODEL FORMULATION

With reference to the geometry of the problem shown in Figure 1, consider unsteady axisymmetric flow in the thin gap between a vertically moving rigid impermeable surface $z = h(r,t)$, referred to hereafter as the "bearing", and a stationary flat rigid impermeable surface at $z = -H_{\rm p}$ coated with a thin rigid porous layer of constant permeability k, porosity ϕ $(0 < \phi < 1)$ and thickness $H_{\rm p}$, referred to hereafter as the "porous bed", where (r,θ,z) denotes the natural cylindrical polar coordinate system with the z-axis vertically upwards and t denotes time. The fluid layer separating the bearing and the porous bed (*i.e.* the region $0 \le z \le h(r,t)$) is

filled with, and the porous bed (*i.e.* the region $-H_\mathrm{p} \le z \le 0$) is saturated with, an incompressible Newtonian fluid of constant density ρ and viscosity μ. The load acting vertically downwards through the bearing, denoted by $L = L(t)$ in Figure 1, may, in general, be prescribed as a function of t. However, for simplicity, in the present work we consider only the particular case in which L is a prescribed constant force.

The thickness of the fluid layer is given by

$$h(r,t) = h_\mathrm{min}(t) + H(r), \tag{1}$$

where $h_\mathrm{min} = h_\mathrm{min}(t)$ is the (unknown) minimum fluid layer thickness and $H = H(r) \ge 0$, with $H(0) = 0$, is the (prescribed) shape of the bearing. The initial minimum fluid layer thickness is denoted by $h_\mathrm{min}(0) = H_\mathrm{f}\,(> 0)$. Following Stone[10], Skotheim and Mahadevan[17] and Ramon *et al.*[15], we consider smooth axisymmetric shapes of the form

$$H(r) = \frac{\mathcal{R}}{2n}\left(\frac{r}{\mathcal{R}}\right)^{2n}, \tag{2}$$

where $\mathcal{R}$ is a radial distance associated with the bearing and the exponent $n \ge 1$ is an integer. As n increases $H(r)$ becomes flatter for $0 \le r \le \mathcal{R}$ and steeper for $r > \mathcal{R}$, and thus in the limit $n \to \infty$ the bearing given by (2) approaches a flat disc of radius $\mathcal{R}$, *i.e.* $H(r) = 0$ for $0 \le r \le \mathcal{R}$, and we recover the problem treated by Knox *et al.*[1].

A. Governing Equations

1. Lubrication Equations

We assume that the fluid layer and the porous bed are of comparable thickness (*i.e.* that H_f and H_p are of the same order of magnitude) and that the aspect ratio of both, namely $\epsilon = H_\mathrm{p}/l \ll 1$, and the (reduced) Reynolds number for the flow in the fluid layer, namely $R^* = \epsilon^2 \rho V l/\mu \ll 1$, where l is the characteristic radial length scale and V is the characteristic radial fluid velocity scale, are both small. The flow in the fluid layer satisfies the continuity and Navier–Stokes equations, and at leading order in the thin-film limit $\epsilon \to 0$ these reduce to the classical lubrication equations,

$$\nabla \cdot \mathbf{v} = 0, \quad \frac{\partial p}{\partial r} = \mu \frac{\partial^2 v_r}{\partial z^2}, \quad \frac{\partial p}{\partial z} = 0, \tag{3}$$

where $\mathbf{v} = (v_r, 0, v_z)$ is the fluid velocity and $p = p(r,t)$ is the fluid pressure.

2. Darcy's Law

The flow in the porous bed satisfies the continuity equation and Darcy's law,

$$\nabla \cdot \mathbf{u} = 0, \quad \mathbf{u} = -\frac{k}{\mu}\nabla P, \tag{4}$$

where $\mathbf{u} = (u_r, 0, u_z)$ is the Darcy velocity and $P = P(r,z,t)$ is the pore pressure. Since the aspect ratio for the porous bed, namely $\epsilon = H_\mathrm{p}/l \ll 1$, is assumed to be small, it can be shown (see, for example, Knox *et al.*[1] and Hicks and Purvis[18]) that at leading order in the limit $\epsilon \to 0$ the solution of (4), subject to no-penetration and continuity of normal stress boundary conditions at $z = -H_\mathrm{p}$ and $z = 0$, respectively, is

$$P = p(r,t), \quad \mathbf{u} = (u_r, 0, u_z) = \frac{k}{\mu}\left(-\frac{\partial p}{\partial r}, 0, \frac{H_\mathrm{p} + z}{r}\frac{\partial}{\partial r}\left(r\frac{\partial p}{\partial r}\right)\right). \tag{5}$$

3. Load Condition

Neglecting inertial terms, the net force exerted on the bearing by the fluid must be equal to the prescribed load L. Hence at leading order in the limit $\epsilon \to 0$ the load condition is

$$2\pi \int_0^\infty pr \, \mathrm{d}r = L. \tag{6}$$

4. Boundary and Initial Conditions

On the lower surface of the bearing the usual no-slip and no-penetration conditions are

$$v_r = 0 \quad \text{and} \quad v_z = \frac{\mathrm{d}h_{\min}}{\mathrm{d}t} \quad \text{on} \quad z = h. \tag{7}$$

On the upper surface of the porous bed mass conservation requires that

$$v_z = u_z \quad \text{on} \quad z = 0. \tag{8}$$

In addition, on this interface we allow for velocity slip with slip length $l_\mathrm{s} = k^{1/2}/\alpha$ as described by the Beavers–Joseph boundary condition

$$\frac{k^{1/2}}{\alpha}\frac{\partial v_r}{\partial z} = v_r - u_r \quad \text{on} \quad z = 0, \tag{9}$$

where $\alpha\,(>0)$ is the dimensionless Beavers–Joseph constant (see, for example, Beavers and Joseph[19] and Nield[20]).

In the far field the pressure in the fluid layer takes its ambient value, which, without loss of generality, we may take to be zero, *i.e.*

$$p \to 0 \quad \text{as} \quad r \to \infty, \tag{10}$$

and on the axis of symmetry we impose the smoothness condition

$$\frac{\partial p}{\partial r} = 0 \quad \text{at} \quad r = 0. \tag{11}$$

The initial condition for the minimum fluid layer thickness is simply

$$h_{\min}(0) = H_\mathrm{f}. \tag{12}$$

B. Non-dimensionalisation

We scale and non-dimensionalise the problem described in Subsection II A using the characteristic radial length scale $l = \mathcal{R}(2nH_\mathrm{p}/\mathcal{R})^{1/2n}$ and the characteristic radial velocity scale $V = LH_\mathrm{p}^2/\mu l^3$ as follows:

$$\begin{gathered}
r = \mathcal{R}\left(\frac{2nH_\mathrm{p}}{\mathcal{R}}\right)^{1/2n} r', \quad z = H_\mathrm{p} z', \quad t = \frac{\mu\mathcal{R}^4}{LH_\mathrm{p}^2}\left(\frac{2nH_\mathrm{p}}{\mathcal{R}}\right)^{2/n} t', \\
h = H_\mathrm{p} h', \quad h_{\min} = H_\mathrm{p} h'_{\min}, \quad H = H_\mathrm{p} H', \quad k = H_\mathrm{p}^2 k', \\
v_r = \frac{LH_\mathrm{p}^2}{\mu\mathcal{R}^3}\left(\frac{2nH_\mathrm{p}}{\mathcal{R}}\right)^{-3/2n} v'_r, \quad v_z = \frac{LH_\mathrm{p}^3}{\mu\mathcal{R}^4}\left(\frac{2nH_\mathrm{p}}{\mathcal{R}}\right)^{-2/n} v'_z, \quad u_r = \frac{LH_\mathrm{p}^2}{\mu\mathcal{R}^3}\left(\frac{2nH_\mathrm{p}}{\mathcal{R}}\right)^{-3/2n} u'_r, \\
u_z = \frac{LH_\mathrm{p}^3}{\mu\mathcal{R}^4}\left(\frac{2nH_\mathrm{p}}{\mathcal{R}}\right)^{-2/n} u'_z, \quad p = \frac{L}{\mathcal{R}^2}\left(\frac{2nH_\mathrm{p}}{\mathcal{R}}\right)^{-1/n} p', \quad P = \frac{L}{\mathcal{R}^2}\left(\frac{2nH_\mathrm{p}}{\mathcal{R}}\right)^{-1/n} P',
\end{gathered} \tag{13}$$

where dimensionless quantities are denoted by a prime ($'$).

Note that since the characteristic radial length scale l depends on n, the characteristic time, velocity and pressure scales also depend on n. This can be inconvenient as it means that it is difficult to compare the (dimensionless) solutions for these variables for different values of n. To avoid this difficulty we define a second set of dimensionless variables obtained by using the radius $\mathcal{R}$ (which is independent of n) to be the characteristic radial length scale, namely

$$\begin{gathered} r = \mathcal{R}\bar{r}', \quad z = H_{\mathrm{p}} z', \quad t = \frac{\mu \mathcal{R}^4}{L H_{\mathrm{p}}^2}\bar{t}', \quad h = H_{\mathrm{p}} h', \quad h_{\min} = H_{\mathrm{p}} h'_{\min}, \quad H = H_{\mathrm{p}} H', \quad k = H_{\mathrm{p}}^2 k', \\ v_r = \frac{L H_{\mathrm{p}}^2}{\mu \mathcal{R}^3}\bar{v}'_r, \quad v_z = \frac{L H_{\mathrm{p}}^3}{\mu \mathcal{R}^4}\bar{v}'_z, \quad u_r = \frac{L H_{\mathrm{p}}^2}{\mu \mathcal{R}^3}\bar{u}'_r, \quad u_z = \frac{L H_{\mathrm{p}}^3}{\mu \mathcal{R}^4}\bar{u}'_z, \quad p = \frac{L}{\mathcal{R}^2}\bar{p}', \quad P = \frac{L}{\mathcal{R}^2}\bar{P}', \end{gathered} \tag{14}$$

which will be used when presenting the results obtained in Sections IV–VI. Henceforth we omit the primes on dimensionless quantities for clarity.

When expressed in terms of the dimensionless variables (13), the continuity and lubrication equations (3), the pore pressure and Darcy velocities (5), the load condition (6), and the boundary and initial conditions (7)–(12) become

$$\frac{1}{r}\frac{\partial}{\partial r}\left(r v_r\right) + \frac{\partial v_z}{\partial z} = 0, \quad \frac{\partial p}{\partial r} = \frac{\partial^2 v_r}{\partial z^2}, \quad \frac{\partial p}{\partial z} = 0, \tag{15}$$

$$P = p(r,t), \quad \mathbf{u} = (u_r, 0, u_z) = k\left(-\frac{\partial p}{\partial r}, 0, \frac{1+z}{r}\frac{\partial}{\partial r}\left(r\frac{\partial p}{\partial r}\right)\right), \tag{16}$$

$$2\pi \int_0^\infty p r \,\mathrm{d}r = 1, \tag{17}$$

$$v_r = 0, \quad v_z = \frac{\mathrm{d}h_{\min}}{\mathrm{d}t} \quad \text{on} \quad z = h, \tag{18}$$

$$v_z = u_z \quad \text{on} \quad z = 0, \tag{19}$$

$$\frac{k^{1/2}}{\alpha}\frac{\partial v_r}{\partial z} = v_r - u_r \quad \text{on} \quad z = 0, \tag{20}$$

$$p \to 0 \quad \text{as} \quad r \to \infty, \tag{21}$$

$$\frac{\partial p}{\partial r} = 0 \quad \text{at} \quad r = 0, \tag{22}$$

$$h_{\min}(0) = d, \quad \text{where} \quad d = \frac{H_{\mathrm{f}}}{H_{\mathrm{p}}}, \tag{23}$$

respectively.

C. Unsteady Reynolds Equation

Solving equations (15a) and (15b) for v_r and v_z subject to (18a), (19) and (20) using (16) yields

$$v_r = -\frac{(h-z)\left[(\alpha h + k^{1/2})z + k^{1/2}(h + 2\alpha k^{1/2})\right]}{2(\alpha h + k^{1/2})}\frac{\partial p}{\partial r}, \tag{24}$$

$$v_z = \frac{\mathcal{F}(h,z)}{12 r(\alpha h + k^{1/2})}\frac{\partial}{\partial r}\left(r\frac{\partial p}{\partial r}\right), \tag{25}$$

where the function $\mathcal{F}(h,z)$ is defined by

$$\mathcal{F}(h,z) = 2(\alpha h + k^{1/2})(6k - z^3) + 3\alpha(h^2 - 2k)z^2 + 6k^{1/2}h(h + 2\alpha k^{1/2})z. \tag{26}$$

Substituting (25) into (18b) we obtain

$$\frac{\mathrm{d}h_{\min}}{\mathrm{d}t} = \frac{1}{12r}\frac{\partial}{\partial r}\left(\frac{r\left[h^2(\alpha h^2 + 4k^{1/2}h + 6\alpha k) + 12k(\alpha h + k^{1/2})\right]}{\alpha h + k^{1/2}}\frac{\partial p}{\partial r}\right), \tag{27}$$

where the fluid layer thickness $h = h(r,t)$ is given by

$$h = h_{\min}(t) + r^{2n}. \tag{28}$$

The unsteady Reynolds equation (27) subject to the load condition (17), the pressure boundary conditions (21) and (22), and the initial condition (23) determine $p = p(r,t)$ and $h_{\min} = h_{\min}(t)$.

III. GENERAL SOLUTION

Solving the unsteady Reynolds equation (27) subject to (21) and (22) yields an expression for the fluid pressure $p = p(r,t)$:

$$p = -6\left(\int_r^\infty \frac{\tilde{r}(\alpha h + k^{1/2})}{h^2(\alpha h^2 + 4k^{1/2}h + 6\alpha k) + 12k(\alpha h + k^{1/2})}\,\mathrm{d}\tilde{r}\right)\frac{\mathrm{d}h_{\min}}{\mathrm{d}t}, \tag{29}$$

where $h = h(\tilde{r},t) = h_{\min}(t) + \tilde{r}^{2n}$. Applying (17) gives rise to a first-order ordinary differential equation for the minimum fluid layer thickness $h_{\min} = h_{\min}(t)$:

$$1 = -6\pi\left(\int_0^\infty \frac{\tilde{r}^3(\alpha h + k^{1/2})}{h^2(\alpha h^2 + 4k^{1/2}h + 6\alpha k) + 12k(\alpha h + k^{1/2})}\,\mathrm{d}\tilde{r}\right)\frac{\mathrm{d}h_{\min}}{\mathrm{d}t}, \tag{30}$$

which when solved subject to (23) yields an explicit expression for the time for $h_{\min}$ to reduce to a given value $t = t(h_{\min})$:

$$t(h_{\min}) = 6\pi\int_{h_{\min}}^d\int_0^\infty \frac{\tilde{r}^3(\alpha h + k^{1/2})}{h^2(\alpha h^2 + 4k^{1/2}h + 6\alpha k) + 12k(\alpha h + k^{1/2})}\,\mathrm{d}\tilde{r}\,\mathrm{d}s, \tag{31}$$

where $h = s + \tilde{r}^{2n}$.

In the case of an impermeable bed, $k = 0$, the solutions for $h_{\min} = h_{\min}(t)$ and $p = p(r,t)$ are given by

$$h_{\min} = \begin{cases} d\exp\left(-\dfrac{2t}{3\pi}\right) & \text{when } n = 1, \\ \dfrac{3\pi d}{3\pi + 4dt} & \text{when } n = 2, \\ \left(d^{-2(n-1)/n} + \dfrac{2n^2\sin(2\pi/n)}{3\pi^2(n-2)}t\right)^{-n/2(n-1)} & \text{when } n \geq 3, \end{cases} \tag{32}$$

and

$$p = \begin{cases} \dfrac{h_{\min}}{\pi(h_{\min} + r^2)^2} & \text{when } n = 1, \\ \dfrac{1}{2\pi h_{\min}^{1/2}}\left[3\tan^{-1}\left(\dfrac{h_{\min}^{1/2}}{r^2}\right) - \dfrac{h_{\min}^{1/2}r^2(5h_{\min} + 3r^4)}{(h_{\min} + r^4)^2}\right] & \text{when } n = 2, \\ \dfrac{2n^3\sin(2\pi/n)h_{\min}^{(3n-2)/n}}{\pi^2(n-1)(n-2)}\displaystyle\int_r^\infty \frac{\tilde{r}}{(h_{\min} + \tilde{r}^{2n})^3}\,\mathrm{d}\tilde{r} & \text{when } n \geq 3. \end{cases} \tag{33}$$

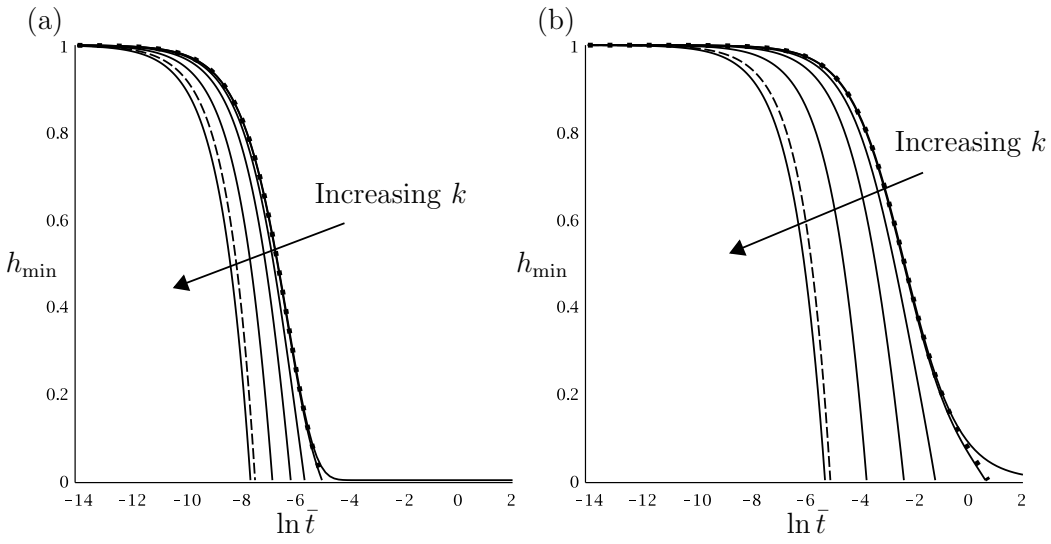

FIG. 2: (a) Plots of $h_{\min}$ given by (31) as a function of $\ln \bar{t}$ for (a) $n = 1$ and (b) $n = 2$ for $k = 0, 10^{-4}, 10^{-2}, 10^{-1}, 1$ and 10 (solid lines), the small-k asymptotic solutions given by (66) for $k = 10^{-4}$ (dotted lines), and the large-k asymptotic solutions given by (A2) for $n = 1$ and (A7) for $n = 2$ for $k = 10$ (dashed lines).

The solution for $h_{\min} = h_{\min}(t)$ given by (32) is equivalent[21] to that given by Stone[10].

In the case of a porous bed, $k \neq 0$, the integrals (29) and (31) were evaluated numerically. (The integral in (31) may, in principle, be evaluated in closed form, but the resulting expression is unwieldy.)

For simplicity, in all of the plots presented in the present work we take $d = 1$ and $\alpha = 1$.

IV. MINIMUM FLUID LAYER THICKNESS AND CONTACT TIME

Figure 2 shows $h_{\min}$ given by (31) plotted as a function of $\ln \bar{t}$ for various values of n and k. Figure 2 shows that increasing k decreases $t(h_{\min})$, *i.e.* decreases the time for the minimum fluid layer thickness to reduce to a given value. Figure 2 also shows that for "small" values of k (specifically, for $k = 0, 10^{-4}, 10^{-2}$ and 10^{-1}) increasing n increases $t(h_{\min})$, whereas for "large" values of k (specifically, for $k = 1$ and 10) increasing n decreases $t(h_{\min})$. Furthermore, Figure 2 shows that when the bed is porous the bearing and the bed always come into contact in a finite time. This finite contact time is denoted by $t_{\rm c}$, and is given by setting $h_{\min} = 0$ in (31) to yield

$$t_{\rm c} = 6\pi \int_0^d \int_0^\infty \frac{\tilde{r}^3(\alpha h + k^{1/2})}{h^2(\alpha h^2 + 4k^{1/2}h + 6\alpha k) + 12k(\alpha h + k^{1/2})} \, {\rm d}\tilde{r} \, {\rm d}s, \tag{34}$$

where again $h = s + \tilde{r}^{2n}$.

Figure 3 shows $\ln \bar{t}_{\rm c}$ given by (34), where $\bar{t}_{\rm c} = (2nH_{\rm p}/\mathcal{R})^{2/n} t_{\rm c}$, plotted as a function of $\ln k$ for various values of n and also, for comparison, the solution for a flat bearing given by equation (4.32) in Knox *et al.*[1]. Figure 3 shows that, in agreement with Figure 2, increasing k decreases $\bar{t}_{\rm c}$, and that when the permeability $k \ll 1$ is small increasing n increases $\bar{t}_{\rm c}$, whereas when the permeability $k \gg 1$ is large increasing n decreases $\bar{t}_{\rm c}$. This latter behaviour is confirmed by the asymptotic solutions in the small-k and the large-k limits given subsequently in Section VII and Appendix A, respectively, which are also shown in Figures 2 and 3. Furthermore, Figure 3 shows that as n increases from $n = 1$ to $n = 10$ the solution for $\ln \bar{t}_{\rm c}$ becomes almost indistinguishable from the solution for a flat bearing. The physical reason for this is simply that, as previously pointed out in Section II, in the limit $n \to \infty$ the shape of the bearing approaches a flat disc.

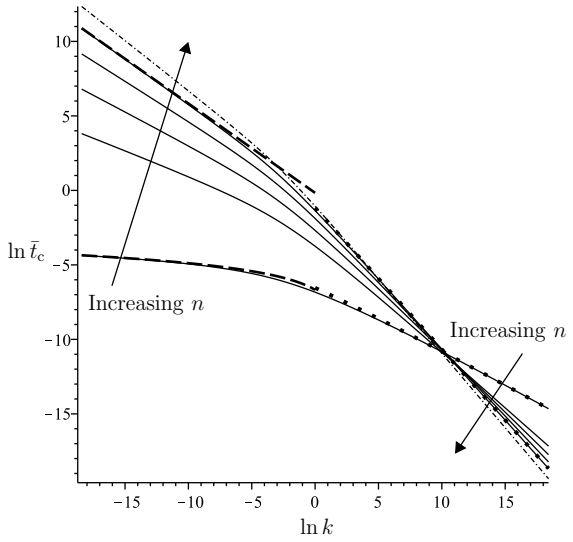

FIG. 3: Plots of $\ln \bar{t}_c$ given by (34) as a function of $\ln k$ for $n = 1, 2, 3, 5$ and 10 (solid lines), the small-k asymptotic solutions given by (60) for $n = 1$ and $n = 10$ (dashed lines), the large-k asymptotic solutions given by (A4) for $n = 1$ and (A8) for $n = 10$ (dotted lines), and the solution for a flat bearing given by equation (4.32) in Knox *et al.*[1] (dash-dotted line).

Figures 4.5–4.7 in Knox[3] (omitted here for brevity) show plots of radial velocity profiles, $\bar{v}_r$ and $\bar{u}_r$, for various values of α, n and k, and instantaneous streamlines for various values of n and k.

V. FLUID PRESSURE

Figure 4 shows $\ln \bar{p}$ given by (29) plotted as a function of $\bar{r}$ for various values of n and k. Figure 4 shows that increasing k decreases the maximum fluid pressure $\bar{p}_{\max} = \bar{p}(0, \bar{t}) = (2nH_p/\mathcal{R})^{-1/n} p_{\max}$ and distributes the fluid pressure $\bar{p}$ over a larger area. Furthermore, Figure 4 shows that increasing k decreases the temporal variations in $\bar{p}$. (In fact, as shown in Appendix A, p is independent of t at leading order in the limit $k \to \infty$.) Figures 4(a)–(d) show that for small values of k (specifically, for $k = 0$ and $k = 10^{-2}$) increasing n decreases $\bar{p}_{\max}$ and distributes $\bar{p}$ over a larger area, whereas Figures 4(e) and 4(f) show that for large values of k (specifically, for $k = 5 \times 10^4$) increasing n increases $\bar{p}_{\max}$ and concentrates $\bar{p}$ over a smaller area. Again, this behaviour is confirmed by the asymptotic solutions in the small-k and large-k limits given subsequently, which are also shown in Figure 4.

Figure 5 shows $\ln \bar{p}_{\max}$ plotted as a function of $\ln \bar{t}$ for various values of n and k. Figure 5 shows that for small values of k the solution for $\bar{p}_{\max}$ as a function of $\bar{t}$ has a maximum turning point. Specifically, $\bar{p}_{\max}$ increases monotonically in time to its maximum value $\bar{p}^\star_{\max}$, which it attains at some time $\bar{t} = \bar{t}^\star$ satisfying $0 < \bar{t}^\star < \bar{t}_c$, and then decreases to its value at $\bar{t} = \bar{t}_c$. The physical reason for this is that, as the asymptotic solutions in the small-k limit given subsequently show, the porous bed is effectively impermeable when $h_{\min} \gg O(k^{1/3})$ is sufficiently large, and the effects of k on $\bar{p}$ become significant only when $h_{\min} = O(k^{1/3})$. Consequently, $\bar{p}_{\max}$ increases monotonically in time when $h_{\min} \gg O(k^{1/3})$, but when $h_{\min} = O(k^{1/3})$ the fluid volume flux into the porous bed is sufficiently large that it causes a decrease in $\bar{p}_{\max}$. Consequently $\bar{p}_{\max} = \bar{p}_{\max}(\bar{t})$ does not attain its maximum value $\bar{p}^\star_{\max}$ when $\bar{t} = \bar{t}_c$. As already mentioned in Section I, a similar observation was made by Goren[13], who found that the maximum value of the force required to pull a sphere away from contact with a thin porous membrane does not occur when the sphere and the membrane are in contact.

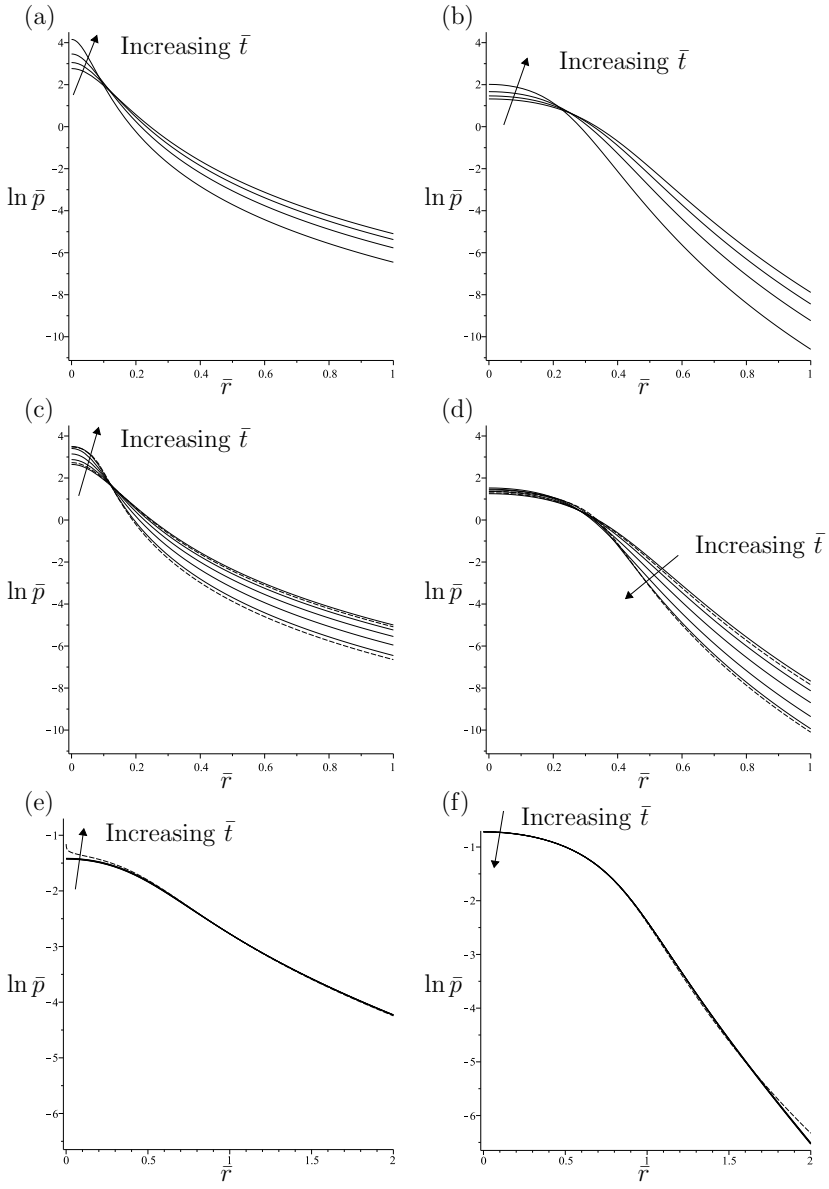

FIG. 4: Plots of $\ln \bar{p}$ given by (29) as a function of $\bar{r}$ at the times when $h_{\min} = d, 3d/4, d/2, d/4$ and 0 (solid lines), the small-k asymptotic solutions given by (64) at the times when $h_{\min} = d$ and 0 in (c) and (d) (dashed lines), and the large-k asymptotic solutions given by (A1) in (e) and (A6) in (f) (dashed lines) for (a) $n = 1$, $k = 0$, (b) $n = 2$, $k = 0$, (c) $n = 1$, $k = 10^{-2}$, (d) $n = 2$, $k = 10^{-2}$, (e) $n = 1$, $k = 5 \times 10^4$, and (f) $n = 2$, $k = 5 \times 10^4$.

VI. FLUID PARTICLE PATHS AND PENETRATION DEPTHS

The path of a fluid particle initially situated at the point (r_0, z_0) (where $r_0 \geq 0$ and $-1 \leq z_0 \leq h(r_0, 0)$) is denoted by (r, z), where $r = r(t)$ and $z = z(t)$ satisfy

$$\frac{\mathrm{d}r}{\mathrm{d}t} = v_r, \quad \frac{\mathrm{d}z}{\mathrm{d}t} = v_z \tag{35}$$

in the fluid layer $0 \leq z \leq h$, and

$$\frac{\mathrm{d}r}{\mathrm{d}t} = \frac{u_r}{\phi}, \quad \frac{\mathrm{d}z}{\mathrm{d}t} = \frac{u_z}{\phi} \tag{36}$$

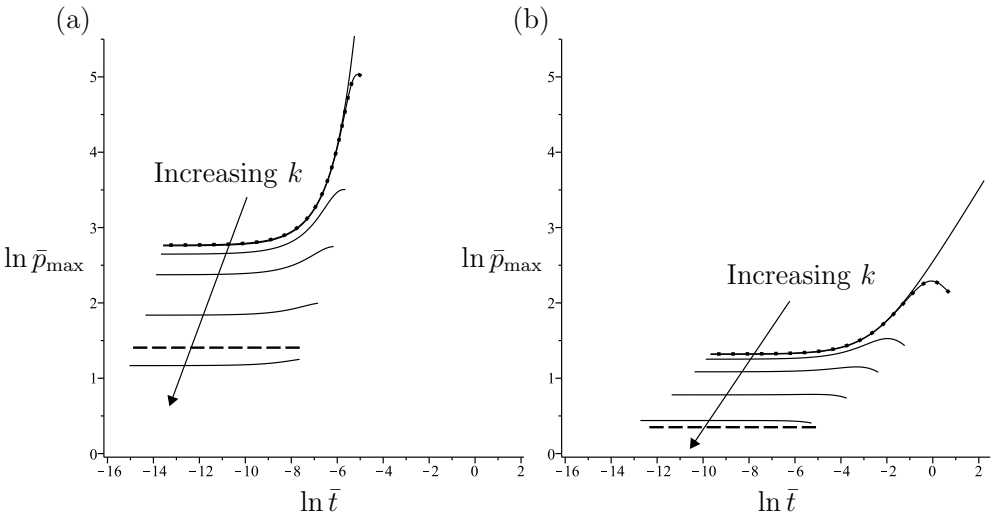

FIG. 5: Plots of $\ln \bar{p}_{\max}$ as a function of $\ln \bar{t}$ for (a) $n = 1$ and (b) $n = 2$ for $k = 0, 10^{-4}, 10^{-2}, 10^{-1}, 1$ and 10 (solid lines), the small-k asymptotic solutions given by (65) for $k = 10^{-4}$ (dotted lines), and the large-k asymptotic solutions given by (A5) for $n = 1$ and (A9) for $n = 2$ for $k = 10$ (dashed lines).

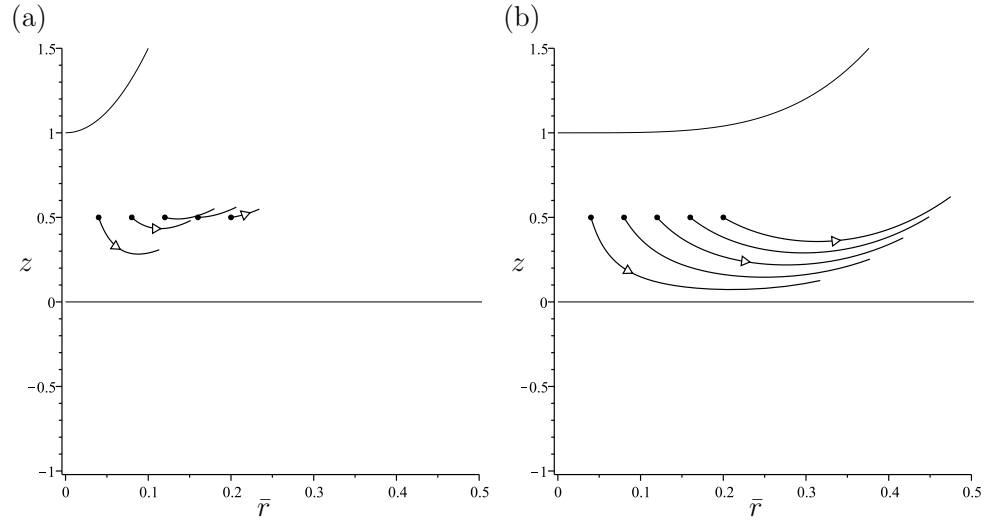

FIG. 6: Plots of the fluid particle paths, $(\bar{r}, z)$, in the case of an impermeable bed, $k = 0$, with $\bar{r} = \bar{r}(h_{\min})$ and $z = z(h_{\min})$ given by (37) and (38) for $(\bar{r}_0, z_0) = (0.04, 0.5)$, $(0.08, 0.5)$, $(0.12, 0.5)$, $(0.16, 0.5)$ and $(0.2, 0.5)$ for (a) $n = 1$ and (b) $n = 2$.

in the porous bed $-1 \le z \le 0$.

Substituting (24), (25) and (29) into (35) and (36) and eliminating t, we obtain the equations

$$\frac{1}{r}\frac{\mathrm{d}r}{\mathrm{d}h_{\min}} = -\frac{3(h-z)[(\alpha h + k^{1/2})z + k^{1/2}(h + 2\alpha k^{1/2})]}{h^2(\alpha h^2 + 4k^{1/2}h + 6\alpha k) + 12k(\alpha h + k^{1/2})}, \tag{37}$$

$$\frac{\mathrm{d}z}{\mathrm{d}h_{\min}} = \frac{1}{2r}\frac{\partial}{\partial r}\left(\frac{\mathcal{F}(h,z)r^2}{h^2(\alpha h^2 + 4k^{1/2}h + 6\alpha k) + 12k(\alpha h + k^{1/2})}\right), \tag{38}$$

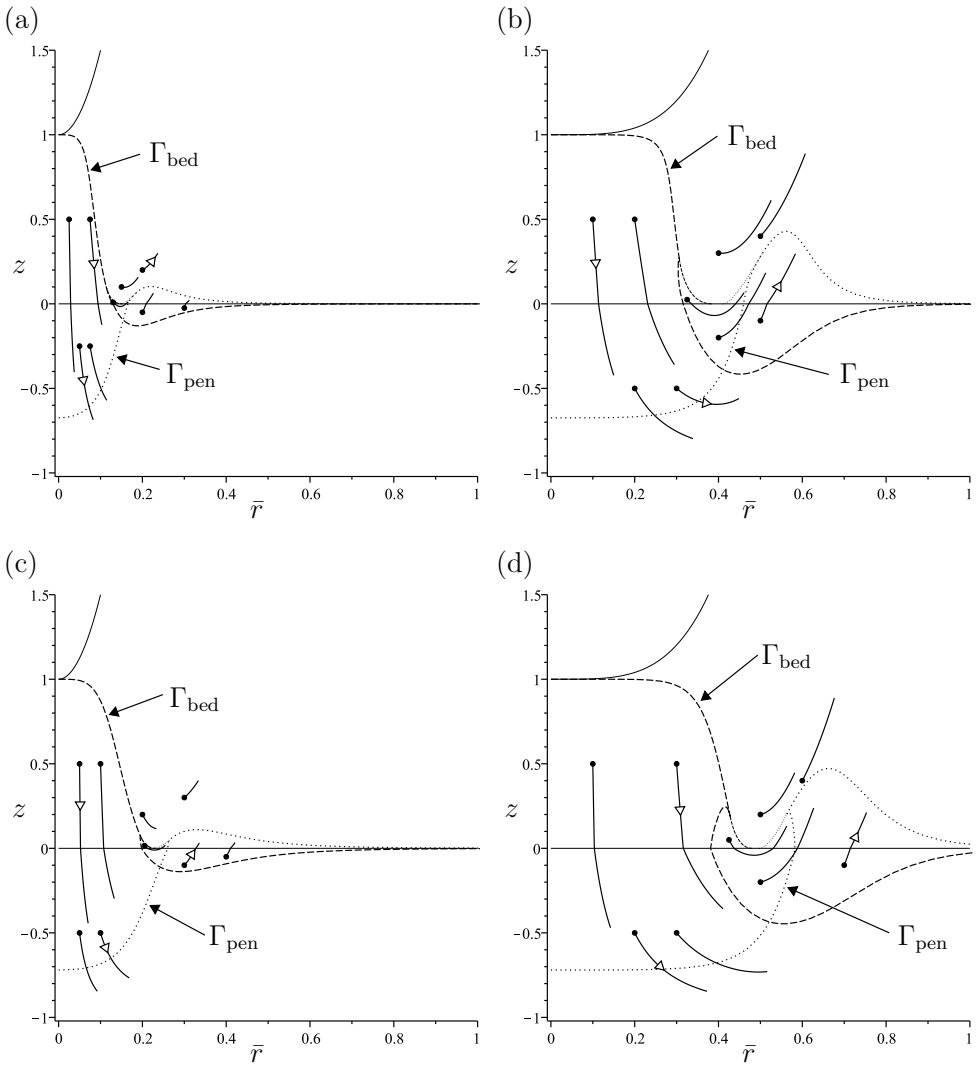

FIG. 7: Plots of the fluid particle paths, $(\bar{r}, z)$, in the case of a porous bed, $k \neq 0$, with $\bar{r} = \bar{r}(h_{\rm min})$ and $z = z(h_{\rm min})$ given by (37)–(40) (solid lines), and plots of the curves $\Gamma_{\rm bed}$ (thick dashed lines), $\Gamma_{\rm pen}$ (thick dotted lines), $\Gamma_{\rm bed^*}$ (thin dashed lines) and $\Gamma_{\rm pen^*}$ (thin dotted lines) for (a) $n = 1$, $k = 0.5$, (b) $n = 2$, $k = 0.5$, (c) $n = 1$, $k = 10$, and (d) $n = 2$, $k = 10$, when $\phi = 3/4$.

in the fluid layer $0 \leq z \leq h$, where the function $\mathcal{F}(h, z)$ is given by (26), and

$$\frac{1}{r}\frac{{\rm d}r}{{\rm d}h_{\rm min}} = -\frac{6k(\alpha h + k^{1/2})}{\phi\left[h^2(\alpha h^2 + 4k^{1/2}h + 6\alpha k) + 12k(\alpha h + k^{1/2})\right]}, \tag{39}$$

$$\frac{1}{1+z}\frac{{\rm d}z}{{\rm d}h_{\rm min}} = \frac{6k}{\phi r}\frac{\partial}{\partial r}\left(\frac{(\alpha h + k^{1/2})r^2}{h^2(\alpha h^2 + 4k^{1/2}h + 6\alpha k) + 12k(\alpha h + k^{1/2})}\right), \tag{40}$$

in the porous bed $-1 \leq z \leq 0$, subject to the initial conditions

$$r = r_0 \quad \text{and} \quad z = z_0 \quad \text{when} \quad h_{\rm min} = d. \tag{41}$$

The equations (37)–(40) were solved numerically.

Figure 6 shows the paths $(\bar{r}, z)$ taken by several fluid particles from their initial positions $(\bar{r}_0, z_0)$, where $\bar{r}_0 = (2nH_{\rm p}/\mathcal{R})^{1/2n} r_0$, in the case of an impermeable bed for $n = 1$ and $n = 2$. In this case the fluid particles are, of course, present in only the fluid layer.

Figure 7 shows the paths taken by several fluid particles in the case of a porous bed for various values of n and k. Figure 7 shows that there are three possible behaviours for the fluid particles that are initially situated in the fluid layer: they can flow through the fluid layer without passing into the porous bed, they can flow from the fluid layer into the porous bed, or they can flow from the fluid layer into the porous bed and then re-emerge into the fluid layer. On the other hand, as Figure 7 also shows, there are only two possible behaviours for the fluid particles initially situated in the porous bed: they can either flow through the porous bed without passing into the fluid layer or they can flow from the porous bed into the fluid layer.

Also plotted in Figure 7 is the curve $\Gamma_{\rm bed}$, which consists of the initial positions $(\bar{r}_0, z_0)$ of the fluid particles that are situated on $z = 0$ when $h_{\min} = 0$, *i.e.* when $\bar{t} = \bar{t}_{\rm c}$. Fluid particles that are initially situated below $\Gamma_{\rm bed}$ are in the porous bed when $\bar{t} = \bar{t}_{\rm c}$, whereas fluid particles that are initially situated above $\Gamma_{\rm bed}$ are in the fluid layer when $\bar{t} = \bar{t}_{\rm c}$. Furthermore, Figure 7 shows that as k increases (with n fixed) or as n increases (with k fixed) the area bounded by the curves $\Gamma_{\rm bed}$, $z = 0$ and $r = 0$ increases, meaning that more fluid flows from the fluid layer into the porous bed. Consequently, mass conservation requires that more fluid flows from the porous bed into the fluid layer and thus the area of the finite region bounded by the curves $\Gamma_{\rm bed}$ and $z = 0$ also increases.

The final positions of the fluid particles that flow from the fluid layer into the porous bed and vice versa are also of interest. Figure 7 also shows the curve $\Gamma_{\rm pen}$, which consists of the final positions $(\bar{r}_{\rm pen}, z_{\rm pen}) = (\bar{r}(0), z(0))$ of the fluid particles initially situated on $z = 0$. The curve $\Gamma_{\rm pen}$ shows the extent to which the fluid particles initially situated in the fluid layer penetrate into the porous bed (the part of the curve below $z = 0$) and the extent to which the fluid particles initially situated in the porous bed can penetrate into the fluid layer (the part of the curve above $z = 0$). In particular, Figure 7 shows that as k increases the fluid particles penetrate deeper and wider into the porous bed. Furthermore, Figure 7 also shows that the fluid particle initially situated at $(\bar{r}_0, z_0) = (0, 0)$ is the one that penetrates deepest into the porous bed. Since both the radial fluid velocity $\bar{v}_r = 0$ at $\bar{r} = 0$ and the radial Darcy velocity $\bar{u}_r = 0$ at $\bar{r} = 0$ are zero for all times, the fluid particles initially situated at $\bar{r} = 0$ move vertically downwards only. Thus setting $r = 0$ in (40) and solving the resulting equation for $z(h_{\min})$ subject to the initial condition $z(d) = 0$ we deduce that the penetration depth $z_{\rm pen}$ of the fluid particle initially situated at $(\bar{r}_0, z_0) = (0, 0)$ is given by

$$z_{\rm pen} = -1 + \exp\left(-\frac{12k}{\phi}\int_0^d \frac{\alpha s + k^{1/2}}{s^2(\alpha s^2 + 4k^{1/2}s + 6\alpha) + 12k(\alpha s + k^{1/2})}\,{\rm d}s\right), \tag{42}$$

which, we note, does not depend on n. Though the maximum penetration depth $z_{\rm pen}$ of fluid particles initially situated in the fluid layer into the porous bed given by (42) does not depend on n, Figure 7 shows that increasing n widens the region over which these fluid particles penetrate into the porous bed and increases the maximum penetration depth $z_{\rm pen}$ of fluid particles initially situated in the porous bed into the fluid layer.

As discussed earlier, the fluid particles that lie above the curve $\Gamma_{\rm bed}$ are situated in the fluid layer when $\bar{t} = \bar{t}_{\rm c}$ (*i.e.* when $h_{\min} = 0$). However, as shown in Figure 7, some of these fluid particles flow from the fluid layer into the porous bed and then re-emerge into the fluid layer. Also shown in Figure 7 is the curve $\Gamma_{\rm bed^*}$, which consists of the initial positions $(\bar{r}_0, z_0)$ of the fluid particles that attain $\bar{v}_z = 0$ on $z = 0$. In particular, the finite region bounded by the curves $\Gamma_{\rm bed}$, $\Gamma_{\rm bed^*}$ and $z = 0$ contains the fluid particles that flow from the fluid layer into the porous bed and then re-emerge into the fluid layer[22]. When $\bar{t} = \bar{t}_{\rm c}$ these fluid particles are situated (in the fluid layer) in the finite region bounded by the curves $\Gamma_{\rm pen}$, $\Gamma_{\rm pen^*}$ and $z = 0$, where the curve $\Gamma_{\rm pen^*}$, which is also plotted in Figure 7, consists of the final positions $(\bar{r}_{\rm pen}, z_{\rm pen})$ of the fluid particles that attain $\bar{v}_z = 0$ on $z = 0$.

VII. LIMIT OF SMALL PERMEABILITY $k \to 0$

In most cases of practical interest the permeabilities of porous media are small, and so in this section we consider the limit of small permeability $k \to 0$. The corresponding analysis of the mathematically interesting but physically less relevant limit of large permeability $k \to \infty$ is given in Appendix A. Specifically, in this Section we show that in the limit $k \to 0$ the contact time is large, and, as in the case of a flat bearing treated by Knox *et al.*[1], regular perturbation solutions for $p = p(r,t)$ and $h_{\min} = h_{\min}(t)$ in powers of $k^{1/2} \ll 1$ are valid only for "short" times $t = O(1)$ when $h_{\min} = O(1)$, and additional asymptotic solutions that are valid for "intermediate" times, when $h_{\min} = O(k^{1/4})$, and "long" times $t = O(t_c)$, when $h_{\min} = O(k^{1/3})$, are required in order to obtain the solution up to $t = t_c$.

For both short and intermediate times the leading order terms in the solutions for $h_{\min} = h_{\min}(t)$ and $p = p(r,t)$ are given by (32) and (33), *i.e.* the solutions in the case $k = 0$, but k and α enter the higher order terms in different ways (see Knox[3] for the details of these higher order terms).

A. Solution for Long Times when $h_{\min} = O(k^{1/3})$

For long times when $h_{\min} = O(k^{1/3})$ we re-scale r, p and $h_{\min}$ and shift (when $n = 1$) or re-scale (when $n \geq 2$) t according to

$$r = (12k)^{1/6n} R, \quad t = \begin{cases} \dfrac{\pi}{2} \ln\left(\dfrac{1}{k}\right) + T & \text{when } n = 1, \\ (12k)^{-2(n-1)/3n} T & \text{when } n \geq 2, \end{cases} \qquad p = (12k)^{-1/3n} P, \quad h_{\min} = (12k)^{1/3} H_{\min}, \tag{43}$$

where R, T, P and $H_{\min}$ are $O(1)$ in the limit $k \to 0$. Seeking a regular perturbation solution to (27), integrated once with respect to r and satisfying (22), of the form

$$P = P_0(R,T) + (12k)^{1/6} P_1(R,T) + O(k^{1/3}) \tag{44}$$

and

$$H_{\min} = H_0(T) + (12k)^{1/6} H_1(T) + O(k^{1/3}), \tag{45}$$

at $O(1)$ and $O(k^{1/6})$ we have

$$\frac{\partial P_0}{\partial R} = \frac{6R}{(H_0 + R^{2n})^3 + 1} \frac{\mathrm{d}H_0}{\mathrm{d}T} \tag{46}$$

and

$$\begin{aligned} \frac{\partial P_1}{\partial R} \;=\; & \frac{3R}{\alpha\left[(H_0 + R^{2n})^3 + 1\right]^2} \left(2\alpha \left[(H_0 + R^{2n})^3 + 1\right] \frac{\mathrm{d}H_1}{\mathrm{d}T} \right. \\ & \left. - \sqrt{3}(1 + 2\sqrt{3}\alpha H_1)(H_0 + R^{2n})^2 \frac{\mathrm{d}H_0}{\mathrm{d}T} \right), \end{aligned} \tag{47}$$

respectively. Solving (46) and (47) subject to $P_0 \to 0$ and $P_1 \to 0$ as $R \to \infty$ yields the solutions

$$P_0 = -6 I_{0,1}(R, H_0, n) \frac{\mathrm{d}H_0}{\mathrm{d}T} \tag{48}$$

and

$$P_1 = -6 I_{0,1}(R, H_0, n) \frac{\mathrm{d}H_1}{\mathrm{d}T} + \frac{3\sqrt{3}(1 + 2\sqrt{3}\alpha H_1)}{\alpha} I_{2,2}(R, H_0, n) \frac{\mathrm{d}H_0}{\mathrm{d}T}, \tag{49}$$

where we have defined the integral

$$I_{M,N}(R,H_0,n)=\int_R^\infty \frac{s(H_0+s^{2n})^M}{[(H_0+s^{2n})^3+1]^N}\,\mathrm{d}s \tag{50}$$

for any n. The solutions P_0 and P_1 must satisfy the load conditions

$$2\pi\int_0^\infty P_0 R\,\mathrm{d}R=1 \quad \text{and} \quad \int_0^\infty P_1 R\,\mathrm{d}R=0 \tag{51}$$

and so at $O(1)$ and $O(k^{1/6})$ we have

$$1=-6\pi J_{0,1}(H_0,n)\frac{\mathrm{d}H_0}{\mathrm{d}T} \tag{52}$$

and

$$J_{0,1}(H_0,n)\frac{\mathrm{d}H_1}{\mathrm{d}H_0}=\frac{\sqrt{3}\left(1+2\sqrt{3}\alpha H_1\right)}{2\alpha}J_{2,2}(H_0,n), \tag{53}$$

respectively, where we have defined the integral

$$J_{M,N}(H_0,n)=\int_0^\infty \frac{s^3(H_0+s^{2n})^M}{[(H_0+s^{2n})^3+1]^N}\,\mathrm{d}s \tag{54}$$

for any n.

Solving (52) and (53) subject to the appropriate matching conditions with the solution that is valid at intermediate times, namely

$$H_0\sim\left\{\begin{array}{cc} \dfrac{d}{12^{1/3}}\exp\left(-\dfrac{2T}{3\pi}\right) & \text{when } n=1\\ \dfrac{3\pi}{4T} & \text{when } n=2\\ \left(\dfrac{3\pi^2(n-2)}{2n^2\sin(2\pi/n)T}\right)^{n/2(n-1)} & \text{when } n\geq 3\end{array}\right\}\to\infty \quad \text{as} \quad T\to\left\{\begin{array}{ll} -\infty & \text{when } n=1,\\ 0 & \text{when } n\geq 2,\end{array}\right. \tag{55}$$

and

$$H_1\to-\frac{1}{2\sqrt{3}\alpha} \quad \text{as} \quad T\to\left\{\begin{array}{ll} -\infty & \text{when } n=1,\\ 0 & \text{when } n\geq 2,\end{array}\right. \tag{56}$$

yields the solutions

$$T=\left\{\begin{array}{ll} \dfrac{\pi}{4}\left(2\ln\left(\dfrac{\mathrm{e}^3d^3}{12}\right)+\displaystyle\sum_{j=1}^3\omega_j(H_0+\omega_j)^2\left(1-2\ln(H_0+\omega_j)\right)\right) & \text{when } n=1,\\ \dfrac{\pi}{2}\displaystyle\sum_{j=1}^3\omega_j(H_0+\omega_j)\left[\ln\left(H_0+\omega_j\right)-1\right] & \text{when } n=2,\\ -\dfrac{\pi^2}{2\sin(2\pi/n)}\displaystyle\sum_{j=1}^3\omega_j(H_0+\omega_j)^{2/n} & \text{when } n\geq 3,\end{array}\right. \tag{57}$$

where

$$\omega_1=1, \quad \omega_2=-\frac{1}{2}(1+\sqrt{3}\mathrm{i}) \quad \text{and} \quad \omega_3=-\frac{1}{2}(1-\sqrt{3}\mathrm{i}) \tag{58}$$

n	1	2	3	5	10	25
$H^\star_{\min}$	0.2478	0.7317	0.8492	0.9363	0.9987	1.0351

TABLE I: The real positive solutions of (61) for $n = 1, 2, \ldots, 25$.

are the cube roots of unity, and

$$H_1 = -\frac{1}{2\sqrt{3}\alpha}. \tag{59}$$

In contrast to the solutions for short and intermediate times, the permeability k appears in the leading order solutions for $p = p(r,t)$ and $h_{\min} = h_{\min}(t)$ at long times, and these solutions remain valid up to $t = t_{\rm c}$, which, in terms of the original variables, is given by

$$t_{\rm c} = \begin{cases} \dfrac{\pi}{2}\ln\left(\dfrac{{\rm e}^{9/2}d^3}{12k}\right) - \dfrac{\pi^2(12k)^{1/6}}{3\alpha} + O(k^{1/3}) & \text{when } \ n = 1, \\ \dfrac{\pi^2\csc[(2+n)\pi/3n]}{2(12k)^{2(n-1)/3n}} - \dfrac{\pi^2\csc(2\pi/3n)}{2\sqrt{3}\alpha n(12k)^{(3n-4)/6n}} + O(k^{-(n-2)/3n}) & \text{when } \ n \geq 2. \end{cases} \tag{60}$$

Note that letting $n \to \infty$ in (60) we recover the solution for a flat bearing obtained by Knox *et al.*[1], and that, as in the case of a flat bearing, the leading-order small-k solution for $t_{\rm c}$ is independent of α. The Beavers–Joseph constant α appears at $O(k^{-(3n-4)/6n})$ in the small-k expansion for $t_{\rm c}$, and inspection of this term shows that increasing α increases $t_{\rm c}$.

The leading-order small-k solution for $p_{\max} = p(0,t)$, given by setting $R = 0$ in (48), has a maximum turning point when $H_0 = H^\star_{\min}$, where $H^\star_{\min}$ is the real positive solution of the equation

$$\left(J_{0,1}(H_0,n)\frac{{\rm d}I_{0,1}(0,H_0,n)}{{\rm d}H_0} - I_{0,1}(0,H_0,n)\frac{{\rm d}J_{0,1}(H_0,n)}{{\rm d}H_0}\right)\bigg|_{H_0=H^\star_{\min}} = 0. \tag{61}$$

Table I contains the real positive solutions of (61) (correct to 4 decimal places) for various values of n. Therefore at leading order in the limit $k \to 0$, and in terms of the original variables, $p_{\max}$ attains its maximum value when

$$h_{\min} = h^\star_{\min} = H^\star_{\min}(12k)^{1/3} \tag{62}$$

which from (43) corresponds to the time

$$t = t^\star = \begin{cases} \dfrac{\pi}{2}\ln(1/k) + T(H^\star_{\min}) & \text{when } \ n = 1, \\ (12k)^{-2(n-1)/3n}T(H^\star_{\min}) & \text{when } \ n \geq 2, \end{cases} \tag{63}$$

where T is given by (57).

B. Uniformly Valid Solutions for $p(r,t)$ and $t(h_{\min})$

A uniformly valid leading order composite solution for $p = p(r,t)$ is given by

$$p(r,t) = \frac{I_{0,1}(R, H_{\min}, n)}{\pi(12k)^{1/3n}J_{0,1}(H_{\min}, n)}, \tag{64}$$

where $R = (12k)^{-1/6n}r$ and $H_{\min} = (12k)^{-1/3}h_{\min}$.

A uniformly valid leading order composite solution for $p_{\max} = p(0,t)$ is given by setting $r = 0$ in (64), which yields

$$p_{\max}(t) = \begin{cases} -\dfrac{\sum_{j=1}^{3} \omega_j \ln(H_{\min}+\omega_j)}{\pi(12k)^{1/3}\sum_{j=1}^{3} \omega_j (H_{\min}+\omega_j)\ln(H_{\min}+\omega_j)} & \text{when } \ n=1, \\ \dfrac{6\sum_{j=1}^{3} \omega_j (H_{\min}+\omega_j)^{-1/2}}{(12k)^{1/6}\sum_{j=1}^{3} \omega_j \ln(H_{\min}+\omega_j)} & \text{when } \ n=2, \\ -\dfrac{2\cos(\pi/n)\sum_{j=1}^{3} \omega_j \left(H_{\min}+\omega_j\right)^{-(n-1)/n}}{\pi(12k)^{1/3n}\sum_{j=1}^{3} \omega_j \left(H_{\min}+\omega_j\right)^{-(n-2)/n}} & \text{when } \ n\geq 3. \end{cases} \tag{65}$$

A uniformly valid leading order composite solution for $t(h_{\min})$ is

$$t(h_{\min}) = \begin{cases} \dfrac{\pi}{4}\left(2\ln\left(\dfrac{\mathrm{e}^3 d^3}{12k}\right) + \sum_{j=1}^{3} \omega_j (H_{\min}+\omega_j)^2\left[1-2\ln(H_{\min}+\omega_j)\right]\right) & \text{when } \ n=1, \\ \dfrac{\pi\left(-3(12k)^{1/3} + 2d\sum_{j=1}^{3} \omega_j (H_{\min}+\omega_j)\left[\ln(H_{\min}+\omega_j)-1\right]\right)}{4d(12k)^{1/3}} & \text{when } \ n=2, \\ \dfrac{\pi^2\left(3(2-n)(12k)^{2(n-1)/3n} - n^2 d^{2(n-1)/n}\sum_{j=1}^{3} \omega_j (H_{\min}+\omega_j)^{2/n}\right)}{2n^2\sin(2\pi/n)\left(12d^3k\right)^{2(n-1)/3n}} & \text{when } \ n\geq 3, \end{cases} \tag{66}$$

where $H_{\min} = (12k)^{-1/3} h_{\min}$. Note that setting $h_{\min} = d$ in (66) yields

$$t(d) = \left\{ \begin{array}{cc} O(k^{1/3}) & \text{when } \ n=1 \\ O(k) & \text{when } \ n\geq 2 \end{array} \right\} \to 0 \quad \text{as} \quad k \to 0, \tag{67}$$

so that at leading order in the limit $k \to 0$ the initial condition (23) is satisfied. Similarly, setting $h_{\min} = 0$ in (66) we see that at leading order in the limit $k \to 0$ it coincides with the leading-order term in (60).

VIII. CONCLUSIONS

In the present work we considered the axisymmetric squeeze-film flow in the thin gap between a stationary flat thin porous bed and a curved impermeable bearing with shape $H \propto r^{2n}$, where n is an integer, moving under a prescribed constant load L.

The unsteady Reynolds equation (27) was solved to yield an explicit solution for the fluid pressure $p(r,t)$ given by (29) in terms of an integral. This solution was then used in the load condition (17) to obtain the equation for the minimum fluid layer thickness $h_{\min}(t)$, which was then solved to obtain an explicit expression for the time for $h_{\min}$ to reduce to a given value $t(h_{\min})$ given by (31) in terms of a double integral.

In contrast to the case of an impermeable bed, when the bed is porous the bearing and the bed always come into contact in a finite contact time t_{c} given by (34). The contact time t_{c} was shown to increase as the permeability k decreases, and, in particular, it was shown in Section VII that in the limit of small permeability $k \to 0$ the contact time

$$t_{\mathrm{c}} = \left\{ \begin{array}{cc} O(\ln(k^{-1})) & \text{when } \ n=1 \\ O(k^{-2(n-1)/3n}) & \text{when } \ n\geq 2 \end{array} \right\} \to \infty \tag{68}$$

is large, and it was shown in Appendix A that in the limit of large permeability $k \to \infty$ the contact time

$$t_{\mathrm{c}} = \left\{ \begin{array}{cc} O(k^{-1/2}\ln k) & \text{when } \ n=1 \\ O(k^{-(2n-1)/2n}) & \text{when } \ n\geq 2 \end{array} \right\} \to 0 \tag{69}$$

is small. For small values of k it was found that increasing n increases t_c, *i.e.* t_c is longer for flatter bearings, whereas for large values of k increasing n decreases t_c, *i.e.* t_c is shorter for flatter bearings. Furthermore, it was shown that, like in the case of a flat bearing, for small values of k the velocity slip on the interface between the fluid and porous layers, introduced via the Beavers–Joseph boundary condition (9) with constant α, has a negligible effect on t_c. In fact, at leading order in the small-k limit the contact time t_c given by (60) is independent of α. However, it was also shown that for large values of k the velocity slip has a significant effect on t_c. In fact, at leading order in the large-k limit the contact time t_c given by (A4) when $n = 1$ and (A8) when $n \geq 2$ depends on α, and, in particular, increasing α decreases t_c.

The fluid pressure p was also calculated. In contrast to the case of an impermeable bed, when the bed is porous p remains finite as the bearing approaches the bed. The maximum fluid pressure $p_{\max}$ was shown to increase as k decreases. In fact, it was shown in Section VII that in the limit of small permeability $k \to 0$ the maximum fluid pressure

$$p_{\max} = O(k^{-1/3n}) \to \infty \tag{70}$$

is large, and it was shown in Appendix A that at leading order in the limit of large permeability $k \to \infty$ the maximum fluid pressure

$$p_{\max} = \left\{ \begin{array}{cc} O(k^{-1/4}(\ln k)^{-1}) & \text{when } n = 1 \\ O(k^{-1/4n}) & \text{when } n \geq 2 \end{array} \right\} \to 0 \tag{71}$$

is small. For small values of k it was found that increasing n decreases $p_{\max}$, *i.e.* for flatter bearings $p_{\max}$ decreases and p is distributed over a larger area, whereas for large values of k increasing n increases $p_{\max}$, *i.e.* for flatter bearings $p_{\max}$ increases and p becomes concentrated over a smaller area. Furthermore, it was shown that for small values of k the maximum value of $p_{\max}$ does not occur when $t = t_c$. The maximum fluid pressure $p_{\max}$ increases monotonically in time to its maximum value $p^\star_{\max}$ which it attains at some time $t = t^\star$ satisfying $0 < t^\star < t_c$ and then decreases to its value at $t = t_c$.

The paths of fluid particles initially situated in both the fluid layer and the porous bed were calculated. It was shown that as k increases the fluid particles that flow from the fluid layer into the porous bed penetrate deeper and wider into the porous bed. It was also shown that, though the maximum penetration depth z_{pen} of these fluid particles given by (42) is independent of n, increasing n widens the region into which these fluid particles penetrate into the porous bed. Furthermore it was shown that, unlike in the case of a flat bearing, there are fluid particles, initially situated in the porous bed, that flow from the porous bed into the fluid layer. In fact, it was shown that there are fluid particles, initially situated in the fluid layer, that flow from the fluid layer into the porous bed and then re-emerge into the fluid layer, and the region in which these fluid particles are initially situated was determined.

Acknowledgements

The first author (DJK) gratefully acknowledges the financial support of the University of Strathclyde via a University Postgraduate Research Scholarship, and the fourth author (SKW) gratefully acknowledges the financial support of the Leverhulme Trust via Research Fellowship RF-2013-355.

---

[1] D. J. Knox, S. K. Wilson, B. R. Duffy, and S. McKee, "Porous squeeze-film flow," IMA J. Appl. Math. **80**, 376–409 (2015).

[2] S. J. Weekley, S. L. Waters, and O. E. Jensen, "Transient elastohydrodynamic drag on a particle moving near a deformable wall," Q. J. Mech. Appl. Math. **59**, 277–300 (2006).
[3] D. J. Knox, *Squeeze-film Flows, with Application to the Human Knee Joint*, PhD thesis, University of Strathclyde (2014).
[4] H. Wu, "A review of porous squeeze films," Wear **47**, 371–385 (1978).
[5] B. N. J. Persson, "Wet adhesion with application to tree frog adhesive toe pads and tires," J. Phys.: Condens. Matter **19**, 376110 (2007).
[6] B. N. J. Persson, "Biological adhesion for locomotion: basic principles," J. Adhesion Sci. Technol. **21**, 1145–1173 (2007).
[7] J. C. Swavola, T. D. Edwards, and M. A. Bevan, "Direct measurement of macromolecule-coated colloid–mucus interactions," Langmuir **31**, 9076–9085 (2015).
[8] H. Brenner, "The slow motion of a sphere through a viscous fluid towards a plane surface," Chem. Eng. Sci. **16**, 242–251 (1961).
[9] R. G. Cox and H. Brenner, "The slow motion of a sphere through a viscous fluid towards a plane surface – II Small gap widths, including inertial effects," Chem. Eng. Sci. **22**, 1753–1777 (1967).
[10] H. A. Stone, "On lubrication flows in geometries with zero local curvature," Chem. Eng. Sci. **60**, 4838–4845 (2005).
[11] H. Wu, "Squeeze-film behaviour for porous annular disks," J. Lubr. Technol **92**, 593–596 (1970).
[12] J. Prakash and S. K. Vij, "Load capacity and time-height relations for squeeze films between porous plates," Wear **24**, 309–322 (1973).
[13] S. L. Goren, "The hydrodynamic force resisting the approach of a sphere to a plane permeable wall," J. Colloid Interface Sci. **69**, 78–85 (1979).
[14] A. Nir, "On the departure of a sphere from contact with a permeable membrane," J. Eng. Math. **15**, 65–75 (1981).
[15] G. Z. Ramon, H. E. Huppert, J. R. Lister, and H. A. Stone, "On the hydrodynamic interaction between a particle and a permeable surface," Phys. Fluids **25**, 073103 (2013).
[16] A. Majhi, T. K. Pardhi, and A. P. Deshpande, "Analysis of squeeze flows of fluids between solid and porous surfaces," Int. J. Multiphase Flow **68**, 93–99 (2015).
[17] J. M. Skotheim and L. Mahadevan, "Soft lubrication: the elastohydrodynamics of nonconforming and conforming contacts," Phys. Fluids **17**, 092101 (2005).
[18] P. D. Hicks and R. Purvis, "Gas-cushioned droplet impacts with a thin layer of porous media," to appear in J. Eng. Math. (2016).
[19] G. S. Beavers and D. D. Joseph, "Boundary conditions at a naturally permeable wall," J. Fluid Mech. **30**, 197–207 (1967).
[20] D. A. Nield, "The Beavers-Joseph boundary condition and related matters: A historical and critical note," Transp. Porous Media **78**, 537–540 (2009).
[21] Note that in the dimensional solution for $h_{\min} = h_{\min}(t)$ given by equation (12) in Stone[10] the exponent of the radius $\mathcal{R}$ is incorrectly given as $3(2n-1)/2n$ when it should in fact be $2(2n-1)/n$.
[22] This behaviour can be more clearly seen in the enlargement of Figure 7 given as Figure 4.13 in Knox[3].

Appendix A: Limit of Large Permeability $k \to \infty$

In this Appendix we show that in the limit of large permeability $k \to \infty$ the contact time is small, and, unlike in the limit of small permeability $k \to 0$ treated in Section VII, there are inner $r = O(k^{1/8n})$ and outer $r = O(k^{1/4n})$ regions in which different (uniformly valid in time) large-k solutions for $p = p(r,t)$ are valid. In the case of a parabolic bearing $n = 1$, the contributions to the normal force exerted on the bearing by the fluid in both the inner and the outer regions are algebraically $O(1)$ and so we must, therefore, obtain the asymptotic solution for $p = p(r,t)$ in both regions in order to obtain the leading order asymptotic solution for $h_{\min} = h_{\min}(t)$. However, for general bearing shapes $H = r^{2n}$ with $n \geq 2$, the contribution to the normal force in the outer region is smaller than the contribution from the inner region, and therefore we need obtain the asymptotic solution for $p = p(r,t)$ only in the inner region in order to obtain the leading order asymptotic

solution for $h_{\min} = h_{\min}(t)$. For brevity, only the main results are summarised here, and further details are given by Knox[3].

1. Parabolic Bearing $n = 1$

A uniformly valid leading order composite solution for $p = p(r,t)$ is

$$p(r,t) = -\frac{1}{8\alpha k}\left[\sqrt{8\alpha}k^{1/4}\tan^{-1}\left(\sqrt{\frac{2}{\alpha}}\frac{k^{1/4}}{r^2}\right) + 48\alpha\int_{r/k^{1/4}}^{\infty}\frac{1+\alpha\tilde{r}^2}{\tilde{r}^3(\alpha\tilde{r}^4+4\tilde{r}^2+6\alpha)}\,\mathrm{d}\tilde{r} - \frac{4k^{1/2}}{r^2}\right]\frac{\mathrm{d}h_{\min}}{\mathrm{d}t}. \tag{A1}$$

Applying the load condition (17) to (A1) and solving the resulting first-order ordinary differential equation for $h_{\min} = h_{\min}(t)$ subject to the initial condition (23) yields

$$t = \frac{\pi(\ln k + g(\alpha))}{8\alpha k^{1/2}}(d - h_{\min}), \quad \textit{i.e.} \quad h_{\min} = d - \frac{8\alpha k^{1/2}}{\pi(\ln k + g(\alpha))}t, \tag{A2}$$

where the function $g = g(\alpha)$ is defined by

$$g(\alpha) = 2\ln(3\alpha) + \frac{4(1-3\alpha^2)}{\sqrt{2(2-3\alpha^2)}}\ln\left(\frac{2-\sqrt{2(2-3\alpha^2)}}{2+\sqrt{2(2-3\alpha^2)}}\right). \tag{A3}$$

Setting $h_{\min} = 0$ in (A2) we obtain the leading order large-k solution for t_{c}:

$$t_{\mathrm{c}} = \frac{\pi d(\ln k + g(\alpha))}{8\alpha k^{1/2}}. \tag{A4}$$

In contrast to the small-k solution, the leading order large-k solution for t_{c} given by (A4) depends on α. Inspection of (A4) shows that increasing α decreases t_{c}. Note that the asymptotic solution for t_{c} given by (A4) is not uniformly valid in the limit $\alpha \to \infty$.

The leading order large-k solution for $p_{\max}$ is

$$p_{\max} = \frac{\sqrt{2\alpha}}{k^{1/4}(\ln k + g(\alpha))}. \tag{A5}$$

2. General Bearing Shapes $n \geq 2$

The leading order solution for $p = p(r,t)$ valid when $r = O(k^{1/8n})$ is

$$p = -\frac{1}{k^{(4n-1)/4n}}\left(\int_{k^{-1/8n}r}^{\infty}\frac{\tilde{r}}{2+\alpha\tilde{r}^{4n}}\,\mathrm{d}\tilde{r}\right)\frac{\mathrm{d}h_{\min}}{\mathrm{d}t}. \tag{A6}$$

There is an outer region $r = O(k^{1/4n})$ in which a different large-k solution for $p = p(r,t)$ is valid. However, the contribution to the normal force exerted on the bearing by the fluid in this outer region is $o(1)$.

Applying the load condition (17) to (A6) and solving the resulting first-order ordinary differential equation for $h_{\min} = h_{\min}(t)$ subject to the initial condition (23) yields

$$t = \frac{\pi^2\csc(\pi/n)}{8nk^{(2n-1)/2n}}\left(\frac{2}{\alpha}\right)^{1/n}(d - h_{\min}), \quad \textit{i.e.} \quad h_{\min} = d - \frac{8n\sin(\pi/n)k^{(2n-1)/2n}}{\pi^2}\left(\frac{\alpha}{2}\right)^{1/n}t. \tag{A7}$$

Setting $h_{\min} = 0$ in (A7) we obtain the leading order large-k solution for t_c:

$$t_c = \frac{\pi^2 d \csc(\pi/n)}{8nk^{(2n-1)/2n}} \left(\frac{2}{\alpha}\right)^{1/n}. \tag{A8}$$

As in the case of a parabolic bearing $n = 1$, when $n \geq 2$ the leading order large-k solution for t_c given by (A8) depends on α, and inspection of (A8) shows that increasing α decreases t_c. Also as in the case of a parabolic bearing $n = 1$, the asymptotic solution for t_c given by (A8) is not uniformly valid in the limit $\alpha \to \infty$. Note that letting $n \to \infty$ in (A8) we recover the solution for a flat bearing obtained by Knox *et al.*[1].

The leading order large-k solution for $p_{\max}$ is

$$p_{\max} = \frac{2\cos(\pi/2n)}{\pi k^{1/4n}} \left(\frac{\alpha}{2}\right)^{1/2n}. \tag{A9}$$